Spring 5-10-2023

De Novo Design of Artificial Cu Peptide for Substrate Oxidation and an Electrochemical Approach to Determine Reorganization Energy

Morgan Murphy

DE NOVO DESIGN OF ARTIFICIAL CU PEPTIDE FOR SUBSTRATE OXIDATION AND AN ELECTROCHEMICAL APPROACH TO DETERMINE REORGANIZATION ENERGY

By
Morgan Murphy

A thesis submitted to the faculty of The University of Mississippi in partial fulfillment of the requirements of the Sally McDonnell Barksdale Honors College

Oxford
May 2023

Approved by:

_____
Advisor: Dr. Saumen Chakraborty

_____
Reader: Dr. Vignesh Sundaresan

_____
Reader: Dr. Kensha Clark

Acknowledgements

The Sally McDonnell Barksdale Honors College
The University of Mississippi, Chemistry Department
The Chakraborty Lab
Divyansh Prakash
Dr. Saumen Chakraborty
Dr. Vignesh Sundaresan
Dr. Kensha Clark
Nikki and Bryan Murphy
All family and friends

Abstract

(Under the direction of Dr. Saumen Chakraborty)

Copper enzymes are found in nature. Their mechanisms and properties are unknown, as spectroscopy is limited. By creating artificially designed copper peptides through de novo design, the behavior, characteristics, and spectroscopy of copper enzymes can be studied to enhance understanding of the mechanisms involved with enzyme catalysis. Design, synthesis, purification, and characterization are completed to create a quality peptide mutant that can be studied to learn about natural enzymes. This plays an important role in pharmaceutical research, renewable energy sourcing, and studies of biological processes in the body. In this study, 3SCC de novo peptide is mutated at different positions, from Ile to Ala, to open the copper active site, allowing for more efficient binding and catalytic activity. Electrochemical and kinetic experiments are currently being conducted to measure catalytic activity at different temperatures to ultimately find the reorganization energy, λ, of the 3SCC and mutants.

Table of Contents

List of Images

List of Tables

List of Figures

Chapter 1: Introduction

1.1 Background

Copper (Cu) metalloproteins are plentiful in nature and perform various functions. Metalloenzymes, like the copper metalloproteins, are structures with metal-bound active sites, in which the metal catalyzes the reaction. For the case of the copper metalloprotein, copper is the metal. Copper is present in the active sites in a multitude of proteins. Type 1 and Type 2 Cu proteins are naturally occurring in biological processes such as the electron transport chain, respiration, oxidative phosphorylation, substrate activation, and redox reactions. There is a lack of spectroscopy of the naturally occurring copper enzymes, and therefore there is much unknown about these enzymes.[6] Artificially designed copper proteins, called de novo artificial proteins, are attractive for research because of their simplicity in structure while offering insight into copper enzyme behavior. They accurately represent the structure and function of the copper enzymes found in nature. By using de novo proteins, the behavior of natural copper enzymes can be studied by learning the mechanisms of the de novo artificial copper peptides under varying conditions.

Class	Catalysis	Cell localization
Laccase	Reduction of O_2 to water	Apoplast
Tyrosinase	Phenol monooxygenation and o-diphenol oxidation	Thylakoid lumen
Plastocyanin	Electron transfer	Thylakoid lumen
Ascorbate oxidase	Enediol oxidation	Apoplast
LPMO	Depolymerization of cellulose through oxidative cleavage	Streptomyces
PHM	Hydroxylation of α-Carbon	Eukaryotes
Tyrosinase	Melanin production catalysis	Melanosomes

Table 1. Naturally Occurring Cu-enzymes in Plants and Nature [6, 7]

Galactose oxidase and lytic polysaccharide monooxygenases (LMPOs) are two naturally occurring copper enzymes. Both are monocopper enzymes. The galactose oxidase oxidizes primary alcohols to aldehydes. LPMO degrades polysaccharides into simple precursors by activating dioxygen to cleave strong C-H bonds. Type 2 Cu proteins are present in substrate activation in which the C-H bond is activated to benzyl alcohol. These copper enzymes are important for biofuel industrial resources as they pertain to renewable energy. Hydrogenase is another metalloenzyme that allows for two-electron reversible conversion of protons to hydrogen, which is a strong source of hydrogen that can be used in energy sourcing. As the burning of nonrenewable fossil fuels as well as the increase in global warming continues, finding alternative sources of energy using natural resources is necessary.[13] De novo designs can be promising in this area, as they function in the same manner as the natural enzyme, producing hydrogen in an artificial manner, which can be used for renewable energy. Furthermore, studying

the behavior of the de novo designed peptides also offers insight into the small molecule drug scaffold that can be used in pharmaceutical research. Scaffolds are what help deliver drugs inside the body, and copper peptides show promise in this area. Copper is a trace element found in the human body and involved in a multitude of biological processes like metabolism and organ function.

The simpler de novo artificial copper peptides provide better understanding of the underlying chemistry of the native enzymes. Through electrochemistry, crystallography, mass spectroscopy, UV-Vis, and more, the structure and function of these copper proteins can accurately be mimicked. This is the motivation for this study.

Chapter 2: De novo protein design, synthesis, purification, and characterization

2.1 De Novo Protein Design

The amino acid sequence of a peptide determines the three-dimensional structure, folding, and function of the protein. Artificial metalloenzymes can be visualized and studied using the de novo design method in which sequences are computationally created. The structure, coordination, interactions, and arrangement of amino acid residues can be observed for multitudes of possible artificial designs, then the synthesis and study of the most accurately mimicked enzyme can begin. De novo design allows researchers to create simpler models of the complex native enzymes. These simpler models share the same structure and function of the naturally occurring ones.

The de novo peptide studied in this project is the trimeric coiled coil, called 3SCC (PDB 7L33), and its mutants. The 3SCC has the sequence $(IAAIKQE)_4$ with a heptad repeat. 3SCC has a nitrogen from one His from each peptide that is connected to a copper. The Ile at the first and fourth positions cause the trimer assembly. 3SCC converts benzyl alcohol to benzaldehyde. 3SCC has already been the subject of multiple publications. In this structure, the Trp is far from the Cu active site, at a length of 28.7 Å. The final sequence of 3SCC is GIAAIKQEHAAIKQEIAAIKQEIAAIKWEG. [9]

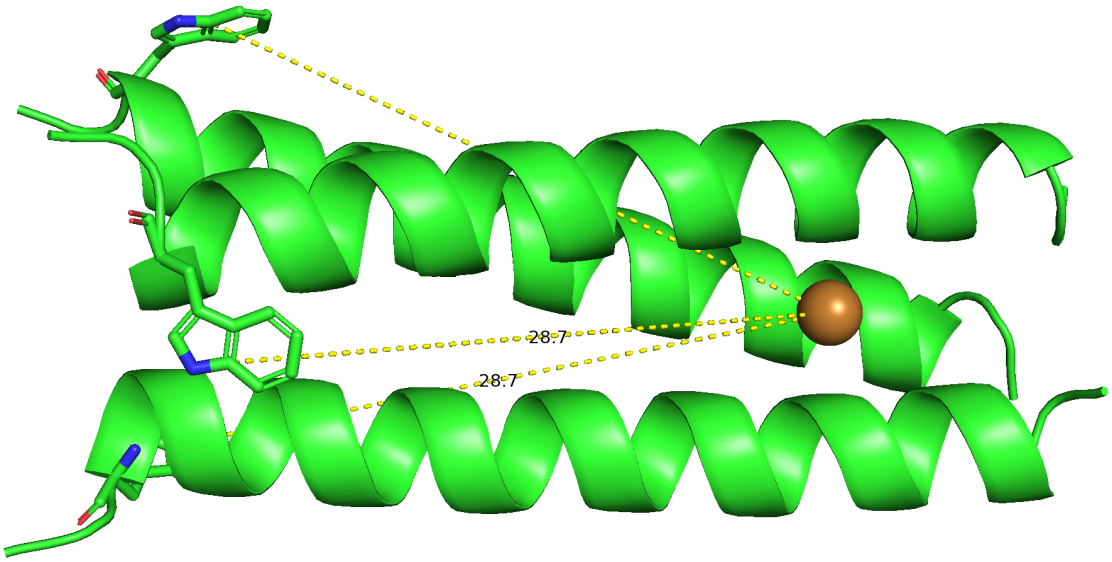

Figure 1. 3SCC drawn in PyMol, side view PDB 7L33

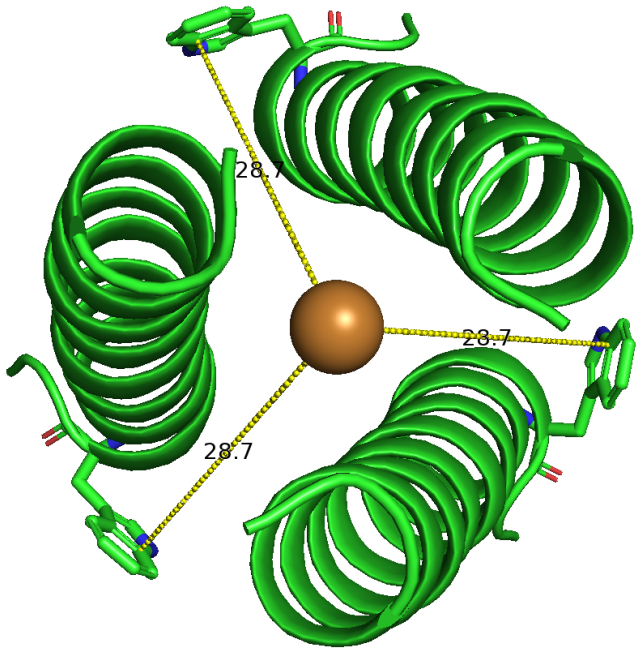

Figure 2. 3SCC drawn in PyMol, top view PDB 7L33

2.2 Synthesis

The synthesis of the 3SCC peptide and mutants was completed through solid phase peptide synthesis by an automated microwave peptide synthesizer, Liberty Blue, CEM.

Image 1. Liberty Blue peptide synthesizer

Rink Amide ProTide Resin on a 0.1 mmol scale was used with a poly(ethylene glycol) polystyrene backbone. The amino acids were weighed in a 30% excess from the recipe produced

by Liberty Blue, then dissolved in Dimethylformamide (DMF). 1 M Oxyma in DMF was the activator base and 0.5 M *N*,*N*′-diisopropylcarbodiimide in DMF was used as the activator. 20% piperidine in DMF was used as the deprotection solution. Cleavage, under the fume hood, of the peptides from the resin and side chain deprotection were achieved by 9.25 mL trifluoroacetic acid (TFA), 0.25 mL each of triisopropylsilane, ethane-1,2-dithiol, and distilled water for 2 hours at room temperature, while stirring. A strong odor is produced, so leaving gloves and other glassware in the hood is necessary for safety. Once the cleavage was complete, the crude peptides were filtered. Then, the peptides were precipitated, washed with cold diethyl ether, dissolved in water, and freeze-dried. Crude peptides are stored in the ultra-low temperature freezer. This is standard procedure for solid phase peptide synthesis. [9]

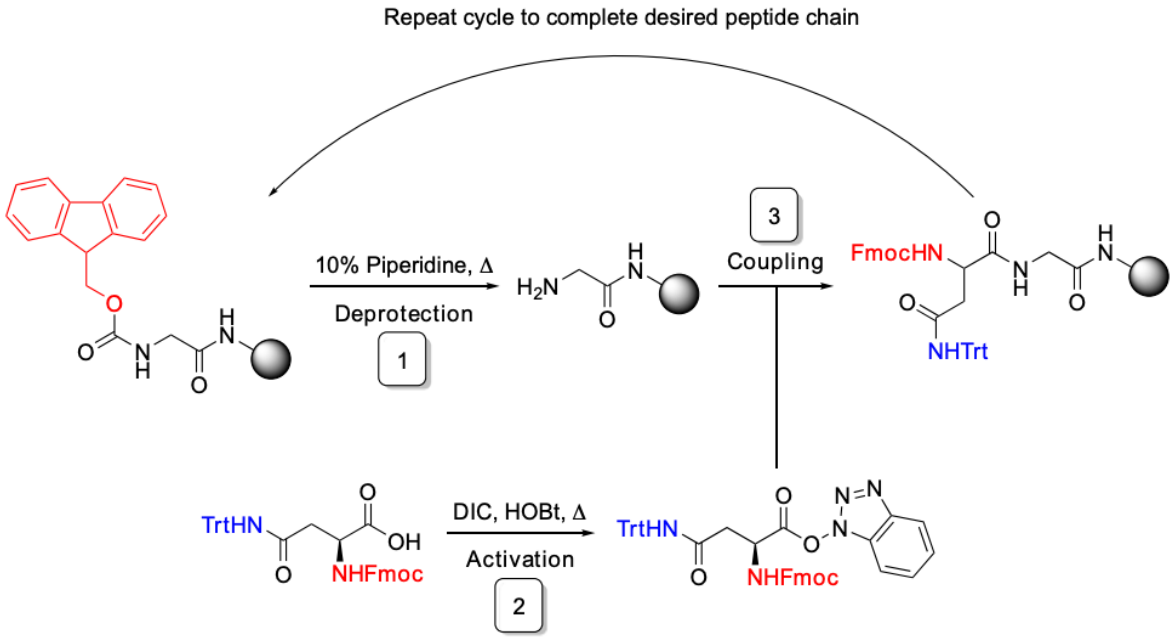

Figure 3. Solid Phase Peptide Synthesis [5]

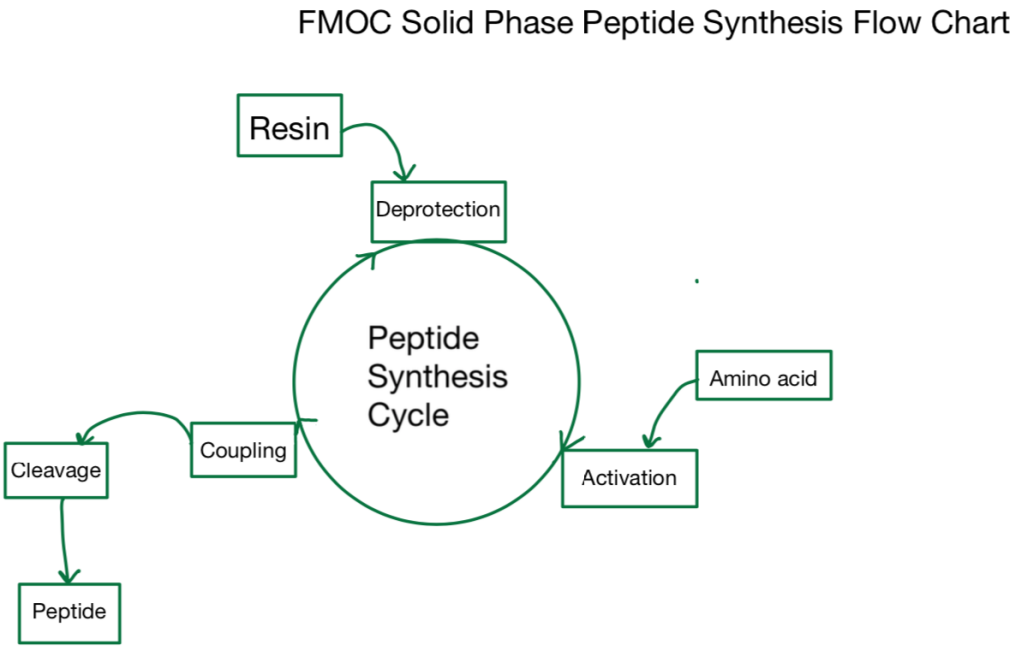

Figure 4. FMOC Solid State Peptide Synthesis Flow Chart [5]

2.3 Purification

The peptides are purified using high performance liquid chromatography. There are two phases in this process, the mobile phase and the stationary phase. When the sample is injected into the column, this is the mobile phase. When the sample is passing through the columns and being separated, this is called the stationary phase. The process relies on adhesion to the column and pressure in order to separate the pure peptide from the other components. HPLC plays a wide range of functions in research, from separating biological components, to pharmaceutical industrial use, to drug testing.

The peptides were dissolved in 10% acetic acid and purified using an Agilent 1260 Infinity II HPLC system. Using a syringe filter, the crude peptide in acetic acid was filtered and stored on ice. In aliquots of 500 µL, the sample of filtered peptide was injected into the HPLC. A

linear gradient from solvent A (1000 µL TFA in 1000 mL H_2O) to solvent B (1000 µL TFA in 900 mL acetonitrile and 100 mL H_2O) was used, following the de novo peptide semi prep method loaded into the online Agilent Infinity application. The peptide was run with 10% B/90% A for 5 min, followed by a linear gradient to 70% B over 25 min at a flow rate of 3 mL/min. The peptide was eluted around 16 minutes after injection. The chromatogram was monitored at 214 and 280 nm.[7, 9]

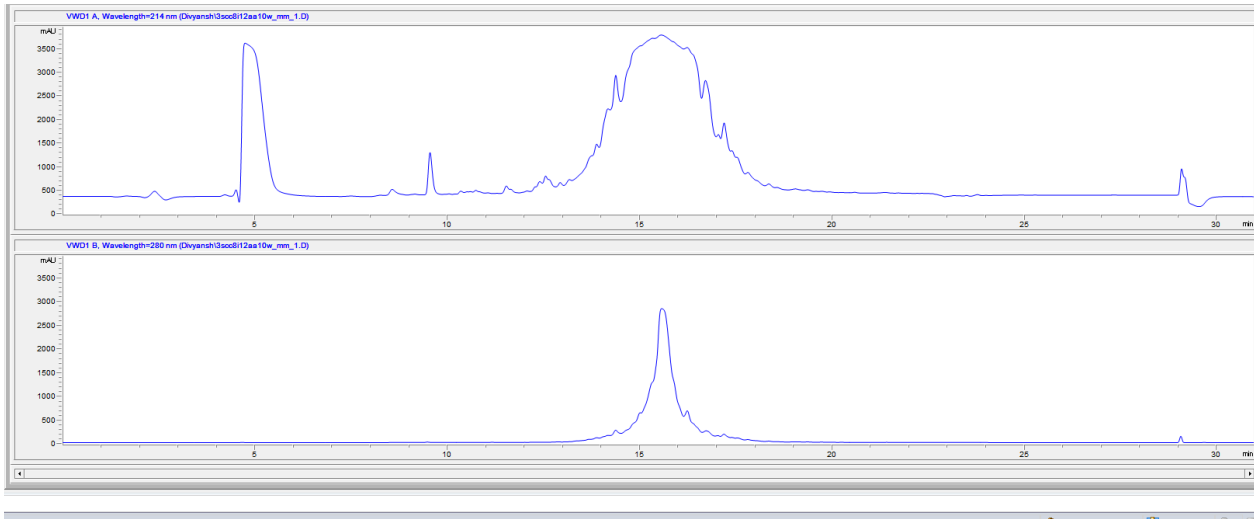

Figure 5. HPLC of I12AA10W, showing elution around 15.7 minutes

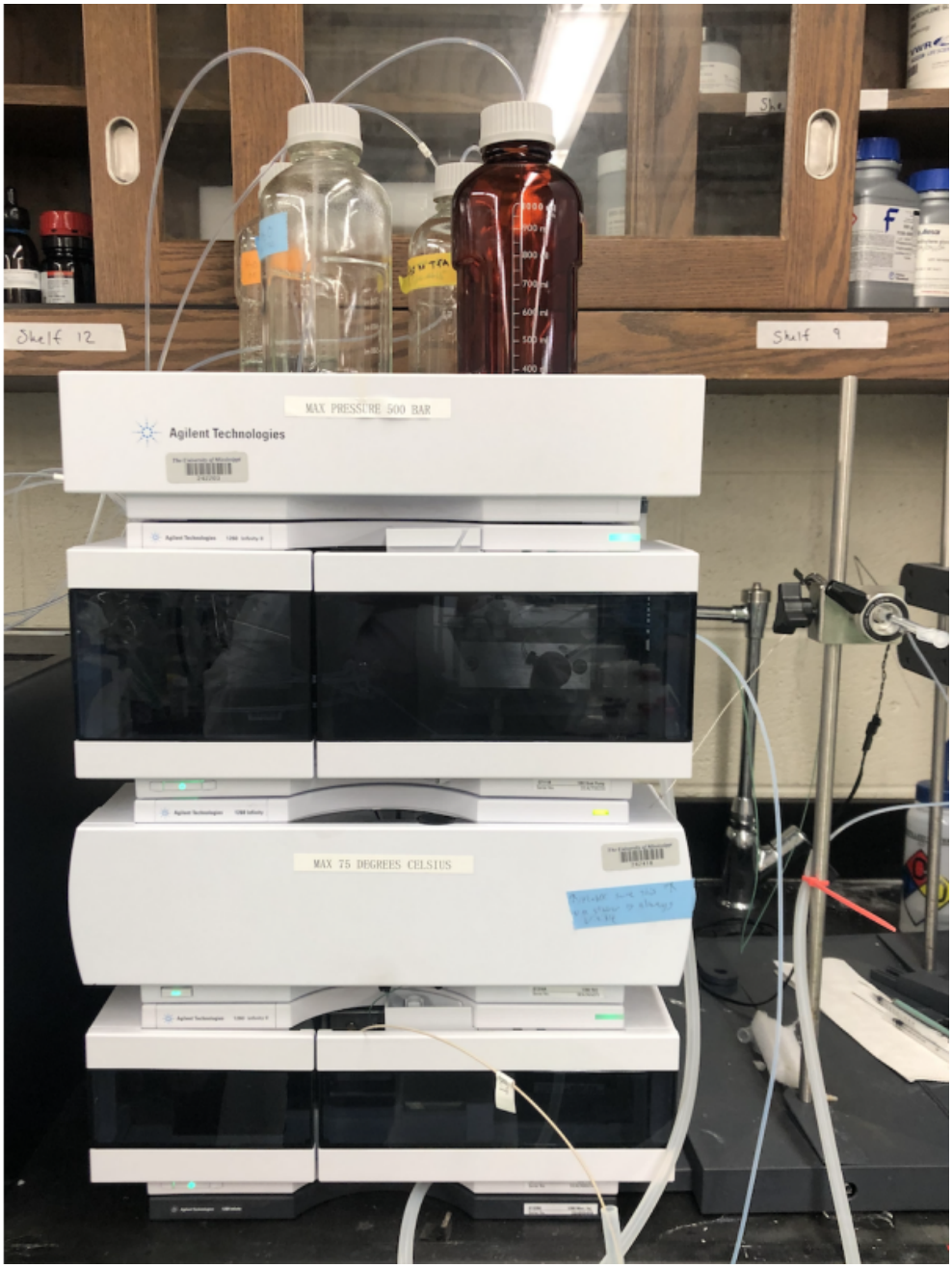

Image 2. Agilent 1260 Infinity II HPLC [7]

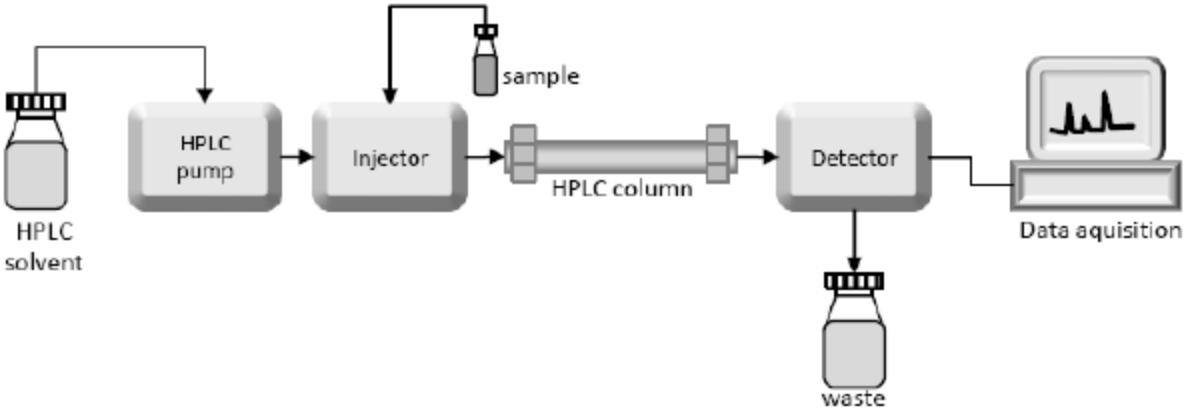

Figure 6. HPLC Schematic [11]

The purified peptide was then poured into a round bottom flask and the acetonitrile solvent was evaporated off using LabTech rotary evaporation with MilliQ water. The purified peptide was freeze dried and stored at −20 °C.

Image 3. LabTech Rotary Evaporator

2.4 Characterization

The 3SCC de novo peptide has been characterized using both spectroscopy and crystallization. The identity of purified peptides is confirmed through MALDI-TOF MS. Crystals were grown by hanging drop method at room temperature, which appeared within two weeks. The solutions for the crystal trays were made through lab standard procedures, from one equivalent of $CuCl_2$ to 40 mg/mL apo peptide dissolved in water. This was then mixed with equal volumes of 0.1 M Tris pH 8.5, 0.2 M MgCl2, and 30% PEG 4000. The crystal trays were greased and covered and allowed to sit in the dark for the crystals to grow, then the trays were analyzed under the microscope, then analyzed at different resolutions for crystal structure. [9, 12]

By analyzing the crystal structure at different resolutions, the quality changes. Lower resolution provides better quality images. Furthermore, the smaller the diffraction Å, the more likely the hydrogen atoms will be seen in the active site. Previous tetramers have been diffracted at 1.2 Å. The hydrogen atom is best seen at diffraction Å of less than 0.9.

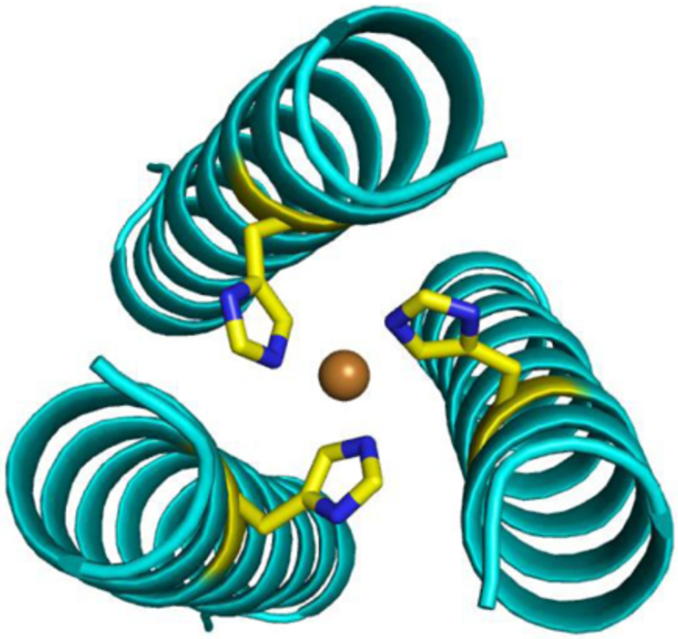

Figure 7. 3SCC peptide crystallized and diffracted to 1.45 Å**,** PyMol PDB 7L33 [9]

Chapter 3: Exploring outer sphere interactions in 3SCC

The sterics of the 3SCC structure impact the de novo peptide's ability for substrate binding (K_M), rate of catalytic activity (k_{cat}), and the catalytic proficiency (k_{cat}/K_M). By altering the sterics of the peptide, the peptide's catalytic efficiency and proficiency can increase.

The original 3SCC structure shows packing in the copper binding site due to the hydrophobic residues of Ile at the d site of the sequence, and this can prevent substrate binding. By mutating the 3SCC from the Ile to Ala at the d site, the active site is opened up, allowing for more binding. The structure of Ala has small methyl side chains that take up less space than the side chains of Ile, which allows more access for substrates to bind to the copper active site.[9, 12] This sequence is the I5A-3SCC mutant with the sequence of GIAAAKQEHAAIKQEIAAIKQEIAAIKWEG. This is seen in C in Figure 8. The other mutant involved in outer sphere interactions is the I12A-3SCC mutant, where the Ile at the 12th position is replaced with Ala. The structure of I12A-3SCC is GIAAIKQEHAAAKQEIAAIKQEIAAIKWEG. This is seen in D in Figure 8.

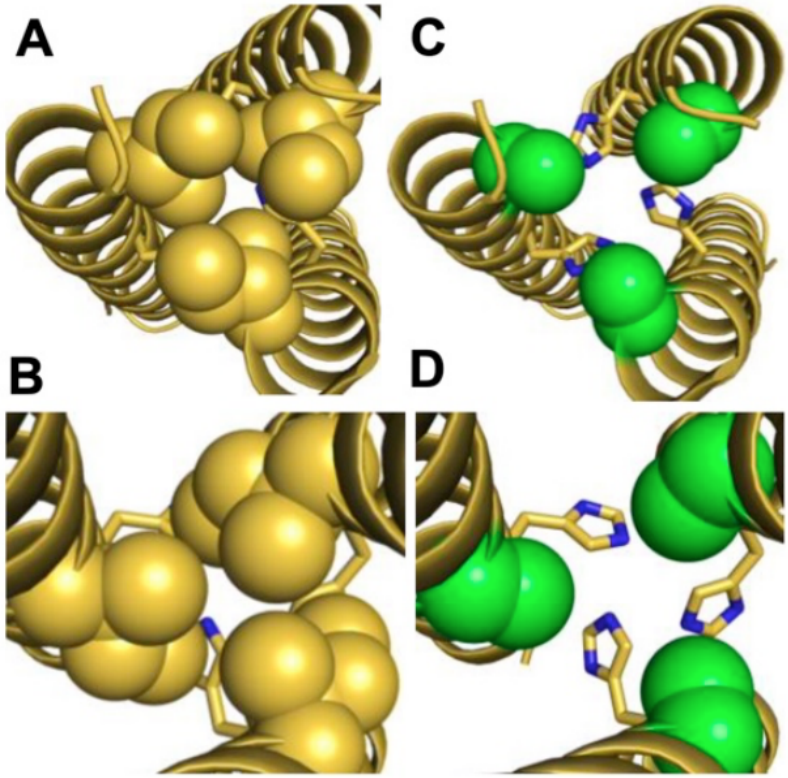

Figure 8. 3SCC with Ile at d sites (A and B) vs. 3SCC with Ala at d sites (C = I5A and D = I12A) [12]

Figure 8 highlights the opening of the active site that occurs with the mutation of Ile to Ala in the I5A-3SCC and I12A-3SCC.

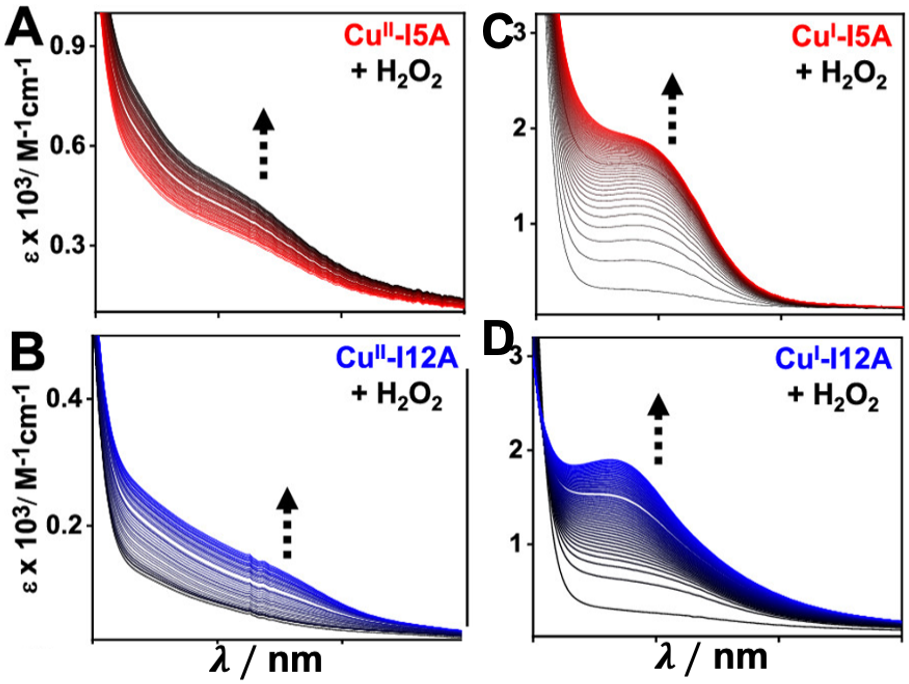

Figure 9. The UV-Vis kinetics of both the I5A-3SCC and I12A-3SCC, kinetics after the addition of 12.5 mM hydrogen peroxide on a time dependent scale. Rates were calculated by taking points from the initial 180 s. Entire experiment duration was 2 hours [12]

In the case of the I5A-3SCC mutant and the I12A-3SCC mutant, the kinetics are an order of magnitude higher for the I12A than the I5A. The initial rates (s^{-1}) of the I5A-3SCC and I12A-3SCC are 8.9 x 10^{-6} and 3.0 x 10^{-5}, respectively.[12] This is because the mutation from Ile to Ala occurs below the His in I12A-3SCC, which allows more space for substrates to bind under the His efficiently. In this case, the substrate is hydrogen peroxide, which results in Cu-O intermediates. Other substrates can also bind to the active site with the newly opened active site, like benzyl alcohol which then converts to benzaldehyde.

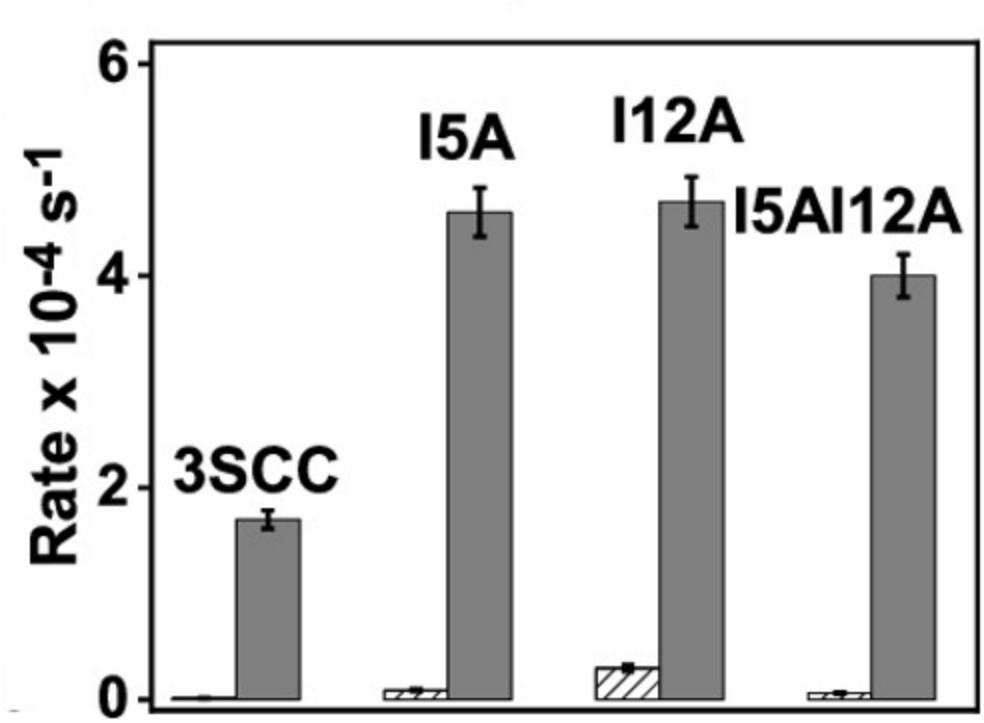

Figure 10. Comparison of Cu^{+} kinetics between 3SCC mutants (gray), striped represents Cu^{2+} kinetics [12]

As seen in Figure 10, the I12A-3SCC mutant has the highest rate of formation of Cu-oxygen species compared to the 3SCC rate of formation. In further comparison of the I5A-3SCC and I12A-3SCC mutants, the λ_{max} values occur at different wavelengths. I5A-3SCC occurs at 365 nm, and I12A-3SCC occurs at 374 nm. The argument that I12A is more kinetically efficient is further corroborated by the production of OH radicals, as seen in Figure 11. [12]

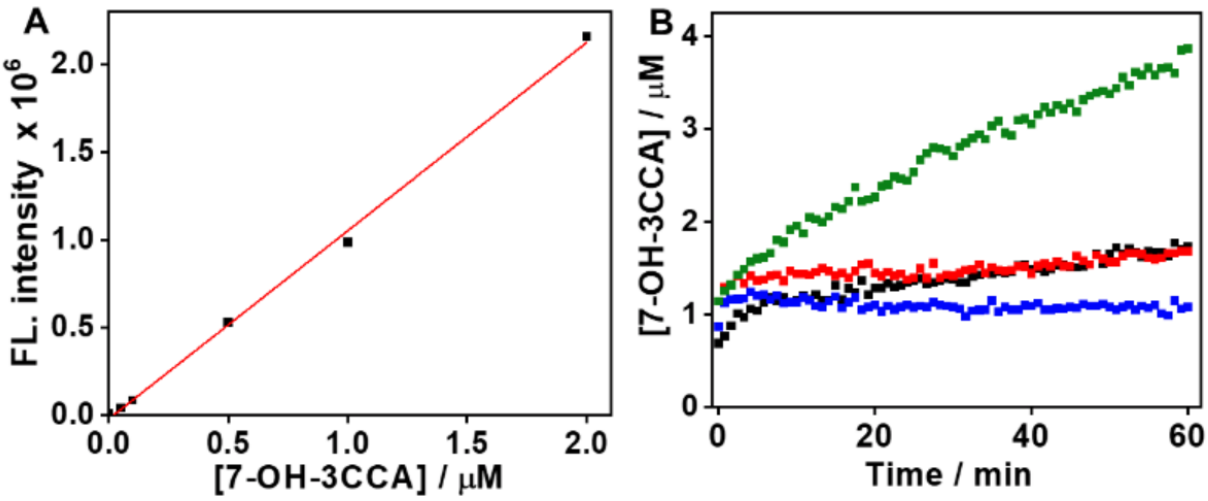

Figure 11. A) Calibration curve of 7-OH-3CCA
B) Production of [OH·] measured by 3CCA assay,
3SCC = black, I5A-3SCC = red, I12A-3SCC = blue [12]

When H_2O_2 was added to the Cu-peptide, OH radicals are produced, producing what is referred to as 7-OH-3CCA. In Figure 11.A), as the concentration of the 7-OH-3CCA increases, fluorescence is directly proportional. In Figure 11.B), the concentration of OH radicals vs time is shown, with the I12A-3SCC producing the lowest concentration of OH radicals over time, suggesting that I12A is the more kinetically favorable mutant. The kinetic favorability is linked to the radical production of the 3SCC mutants in the presence of H_2O_2.

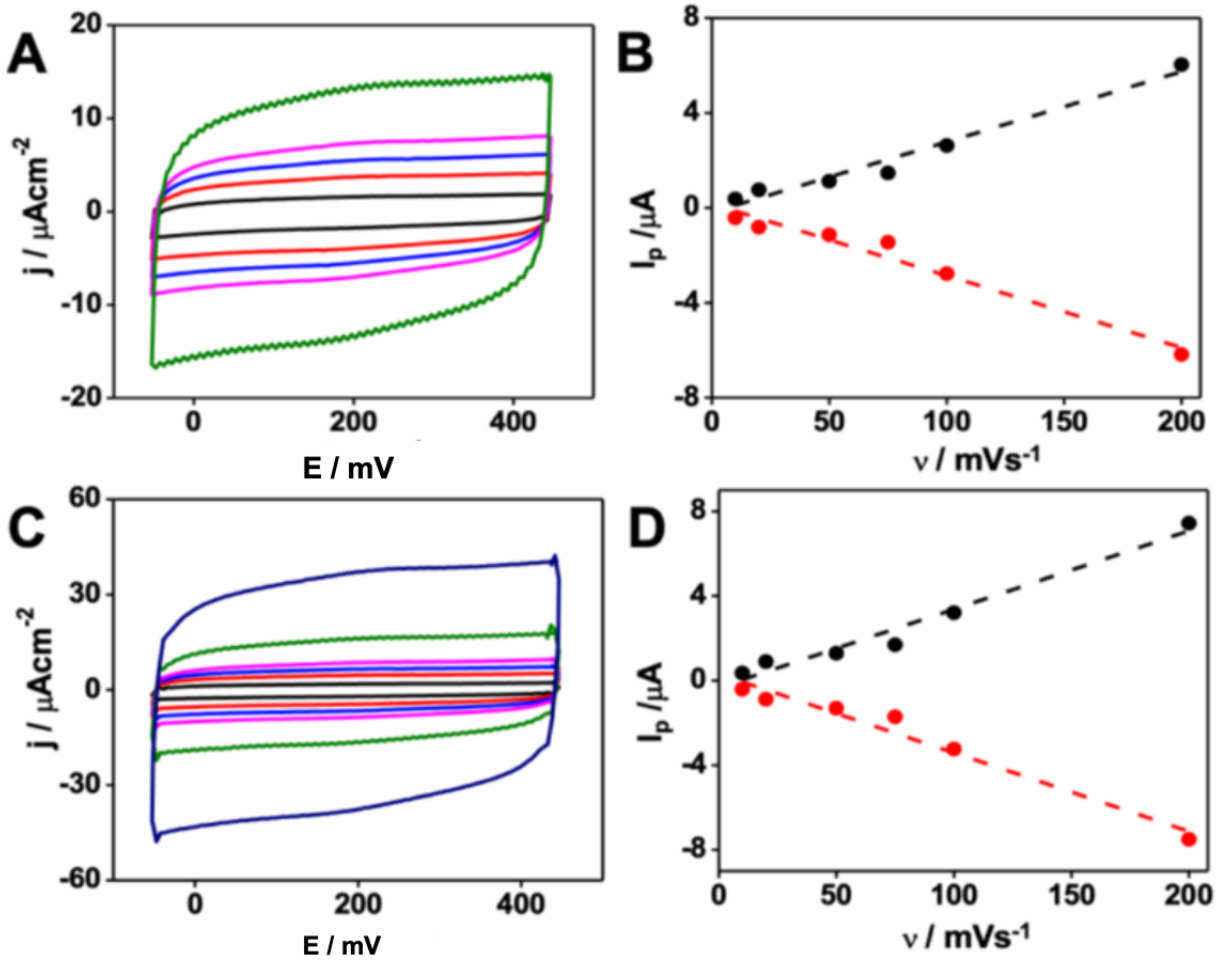

Figure 12. Cyclic Voltammetry (CV) of I5A-3SCC (A) and I12A-3SCC (C) and their correlating **peak current vs scan rate plot (B) and (D)**, respectively
Scan rates = 10 (black), 20 (red), 50 (blue), 75 (magenta), 100 (olive), and 200 (violet) mV/s in 80 mM mixed buffer pH 6.5 [12]

The peak in the direction of 400 → 0 ν/mVs^{-1} is the reduction of the Cu^{2+} to Cu^{+}, and the peak in the opposing direction is the oxidation peak of Cu^{+} to Cu^{2+}. The presence of the peak indicates that not only the copper has binded to the peptide, but also that the redox reactions have occurred. When comparing the CV of the I5A-3SCC mutant to the I12A-3SCC mutant, both show a linear dependence on the scan rate. When the samples are adsorbed on the electrode, the current varies linearly with scan rate. This corroborates the Randels-Sevcik equation, which is

applicable when the sample is dissolved in a buffer, and shows the relationship between peak current, i_p, and scan rate in CV. When the analyte is adsorbed on the surface, a linear dependence is seen between the two. The Randels-Sevcik equation is:

$$i_p = 0.4463\ n^{3/2}\ F^{3/2}\ A\ \frac{D^{1/2} c v^{1/2}}{(RT)^{1/2}}$$

Furthermore, the $E^{0'}$ being positive for both mutants is indicative that the mutants are more stable than the 3SCC parent, with the environment around the active site being more polar. Cu^{2+} is more stable than Cu^{+}.

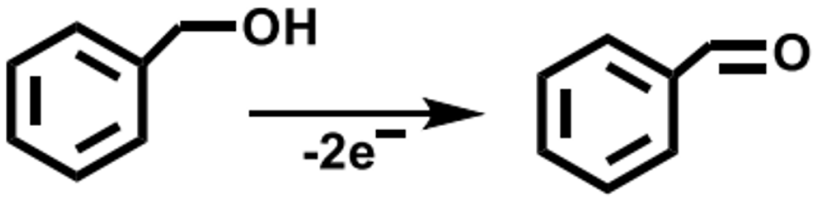

Figure 13. Benzyl alcohol oxidation to benzaldehyde [12]

By observing the oxidation of benzyl alcohol shown in Figure 10 to the benzaldehyde in the presence of different de novo peptides, it is seen that the catalytic efficiency increases when in the mutant form with Ile replaced with Ala at the 5th and 12th position, as opposed to the original 3SCC structure with the bulky active site.

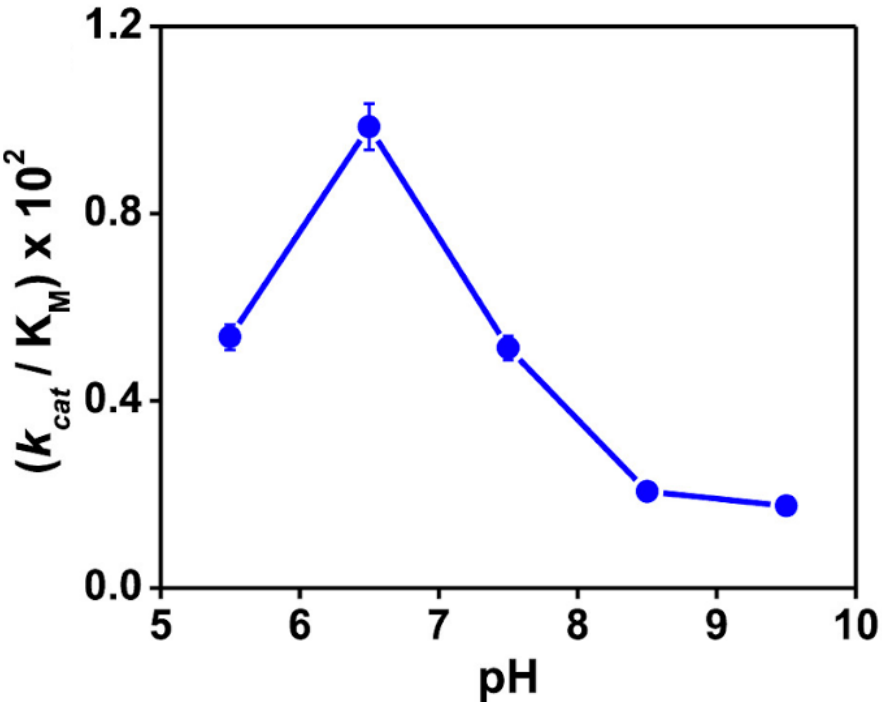

Figure 14. Plot of k_{cat}/K_M vs pH for the electrocatalytic oxidation of benzyl alcohol to benzaldehyde. [12]

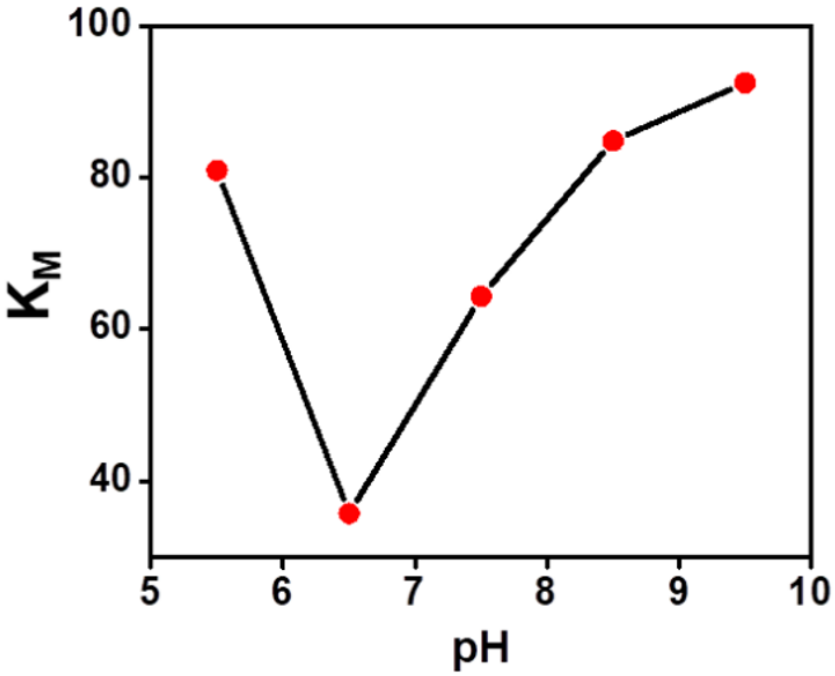

Figure 15. plot of K_M vs pH for electrocatalytic oxidation of benzyl alcohol to benzaldehyde[12]

As seen in Figure 14, the peak of the catalytic efficiency, $k_{cat}/K_{M,}$ is around pH 6.5. In the plot of K_M vs. pH, Figure 15, the lowest K_M value occurs at pH 6.5, so k_{cat}/K_M will have its peak value at pH 6.5 as verified in Figure 14. The K_M and k_{cat} values for both figures were obtained through chronoamperometry (CA) to measure the catalytic activity and efficiency. This shows that at pH 6.5, the mutants are most catalytically favorable, which is significant in understanding the behavior of naturally occurring enzymes.

Chapter 4: Temperature Dependent Studies

4.1 3SCC Mutants

For the study of the mutant strains of 3SCC, mutants were created in PyMol, and their structures were compared to find the most suitable structure. Bringing a Trp from each strand closer to the active site was the desired outcome, as the aromatic side chain of the Trp will stack with Benzene rings of the substrate molecule. This theoretically reduces the K_m value, and therefore makes the peptide more efficient for conversion. Trp is also useful for quantifying proteins using absorbance, at the wavelength of 289 nm. At the 28th position of the 3SCC sequence, Trp is mutated to a Gln. This ion pair forms an assembly. Furthermore, Trp fluoresces in the presence of Cu^+ which offers the ability to study fluorescence as well, in the future.

PyMol was used to visualize the structures of I5A-3SCC Trp mutants, I12A-3SCC Trp mutants, and I5AI12A-3SCC Trp mutants.

Sequence	Name
GIAAIKQEHAAIKQEIAAIKQEIAAIKWEG	3SCC
GIAAAKQEHAAIKQEIAAIKQEIAAIKWEG	I5A
GIAAAKWEHAAIKQEIAAIKQEIAAIKQEG	I5AA7W
GIAAAKQWHAAIKQEIAAIKQEIAAIKQEG	I5AA8W
GIAAAKQEHWAIKQEIAAIKQEIAAIKQEG	I5A10W
GIAAAKQEHAWIKQEIAAIKQEIAAIKQEG	I5AA11W
GIAAIKQEHAAAKQEIAAIKQEIAAIKWEG	I12A
GIAAIKWEHAAAKQEIAAIKQEIAAIKQEG	I12AA7W
GIAAIKQWHAAAKQEIAAIKQEIAAIKQEG	I12AA8W
GIAAIKQEHWAAKQEIAAIKQEIAAIKQEG	I12AA10W
GIAAIKQEHAWAKQEIAAIKQEIAAIKQEG	I12AA11W
GIAAAKQEHAAAKQEIAAIKQEIAAIKWEG	I5AI12A
GIAAAKWEHAAAKQEIAAIKQEIAAIKQEG	I5AI12AA7W
GIAAAKQWHAAAKQEIAAIKQEIAAIKQEG	I5AI12AA8W
GIAAAKQEHWAAKQEIAAIKQEIAAIKQEG	I5AI12AA10W
GIAAAKQEHAWAKQEIAAIKQEIAAIKQEG	I5AI12AA11W

Table 2. Sequences and names of 3SCC mutants

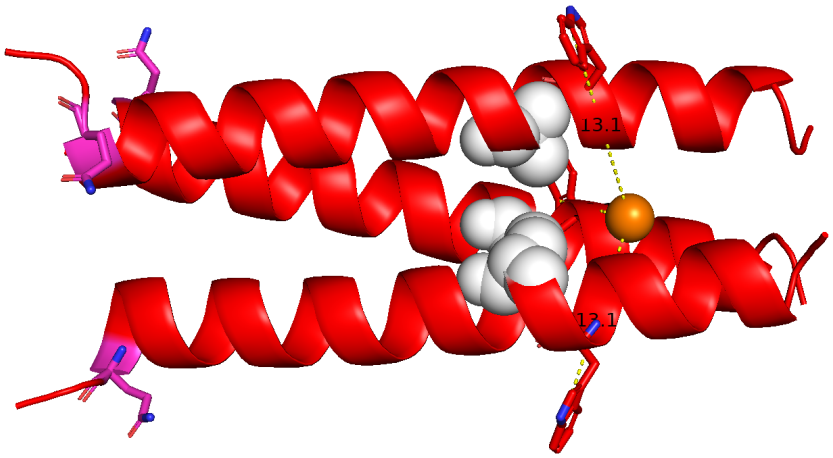

Figure 16. I12AA10W drawn in PyMol, side view

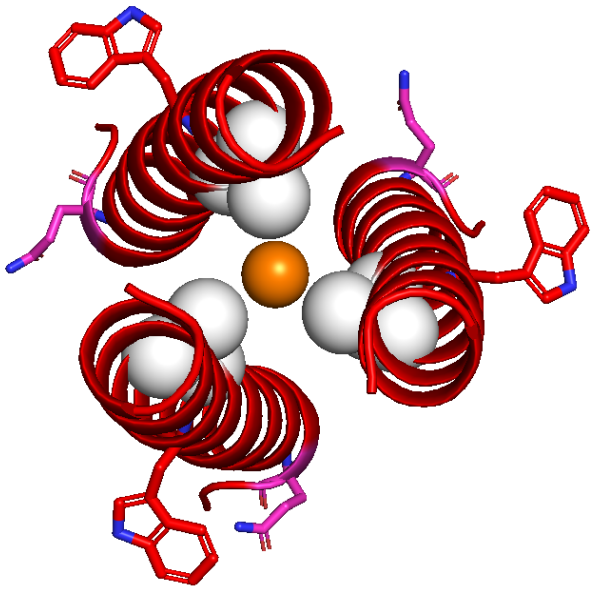

Figure 17. I12AA10W drawn in PyMol, top view

After analyzing the structure and distance between the Trp and the Cu active site, I12AA10W was selected for research. The distance between the Trp and Cu is 28.7 Å in 3SCC. The distance is shortened to 13.1 Å in I12AA10W-3SCC mutant. After selecting this mutant, the peptide was synthesized and purified using the methods in Chapter 2.

Image 4. Crude I12AA10W peptide

To learn more about the 3SCC mutant I12AA10W, temperature dependent studies are currently being conducted to research the reorganization energy of the mutant. The I12AA10W mutant was selected because of the symmetrical structure, the 13.1 Å distance between the Trp and the copper active site, and the orientation of the Trp aromatic side chains which will allow for the stacking with benzene rings of other structures. With the Trp closer to the active site in the mutant than in the original 3SCC, the mutant has fluorescent characteristics. Fluorescence studies are in progress for the reoxidation of H_2O_2 and 3SCC Trp mutants.

Reorganization energy, λ, and the temperature-dependent studies are carried out to calculate the reorganization energy of the de novo peptides.[4] The λ of the system originates from Marcus theory, which is the calculation used to calculate the rate of electron transfer. The lower the reorganization energy, λ, the faster the rate of electron transfer, ET.

Reaction	λ (eV)
azurin (CuII,I)	0.82
plastocyanin (CuII,I)	0.72
nitrite reductase (CuII,I)	0.77
[CuII,I(phen)2]2+/+	2.4
[CuII,I(TMGqu)2]2+/+	0.77
[CuII,I(DMEGqu)2]2+/+	0.89
[LCuIII,II(OH)]0/-	0.95
[CuIII,II(H−2Aib3)]0/−	1.48
[CuII,I(H2TpyNMes)Cl]+/0	1.33
engineered CuA Az	0.4
$Cu_{A\ (blue\ copper)}$ azurin (pH 4.0)	0.75
$Cu_{A\ (blue\ copper)}$ azurin (pH 8.0)	1.07

Table 3. Reorganization energies of naturally occurring copper enzymes and reactions [3]

4.2 Electrochemistry

For the temperature dependent cyclic voltammetry studies, the redox behavior of the mutant was recorded using the Pine Wave Driver 20 and the pyrolytic graphite electrode (PGE) working electrode. The counter electrode was the platinum wire, and the reference electrode was the Ag/AgCl in saturated KCl. All electrochemical experiments were performed under a N_2 gas. Because of the varying temperatures for the experiments, rubber tubing is connected from an aquastat to the glass electrochemical cell. The water temperature is controlled and maintained through this apparatus.

Electrochemistry is a technique used to measure the redox potentials, or electron transfers, of inorganic compounds. The specific method used in this experiment is cyclic

voltammetry, CV. The CV traces, called voltammograms, show current (i) vs potential (E). The peaks seen in the voltammograms are related to the Nernst equation for equilibrium. [1]

The Nernst equation is:

$$E_{cell} = E^0 - (\frac{RT}{nF}) \ln Q$$

In terms of the setup of the electrochemistry, the major parts include the cell, the working electrode, the reference electrode, and the counter electrode. The galvanic cell is a glass chamber filled with a mixed buffer solution. The working electrode, PGE, is the electrode in which the reaction takes place, at the contact of the electrode with the solution. The working electrode must remain meticulously polished to prevent errors or contamination. The polishing method can be found in Figure 18. The reference electrode functions to provide an equilibrium potential for the reaction. In this case it is the Ag/AgCl, in KCl. The potential remains constant so it can serve as a comparison, in these experiments, the reference electrode is the standard hydrogen electrode (SHE). This is where the comparison of "vs. SHE" originates. The counter electrode is to close the circuit of the electronic transfer, to make the circuit complete. Platinum wire is used. When a reduction occurs at the working electrode, the oxidation will occur at the counter electrode. The reactions occur under a gentle flow of N_2 gas. [1]

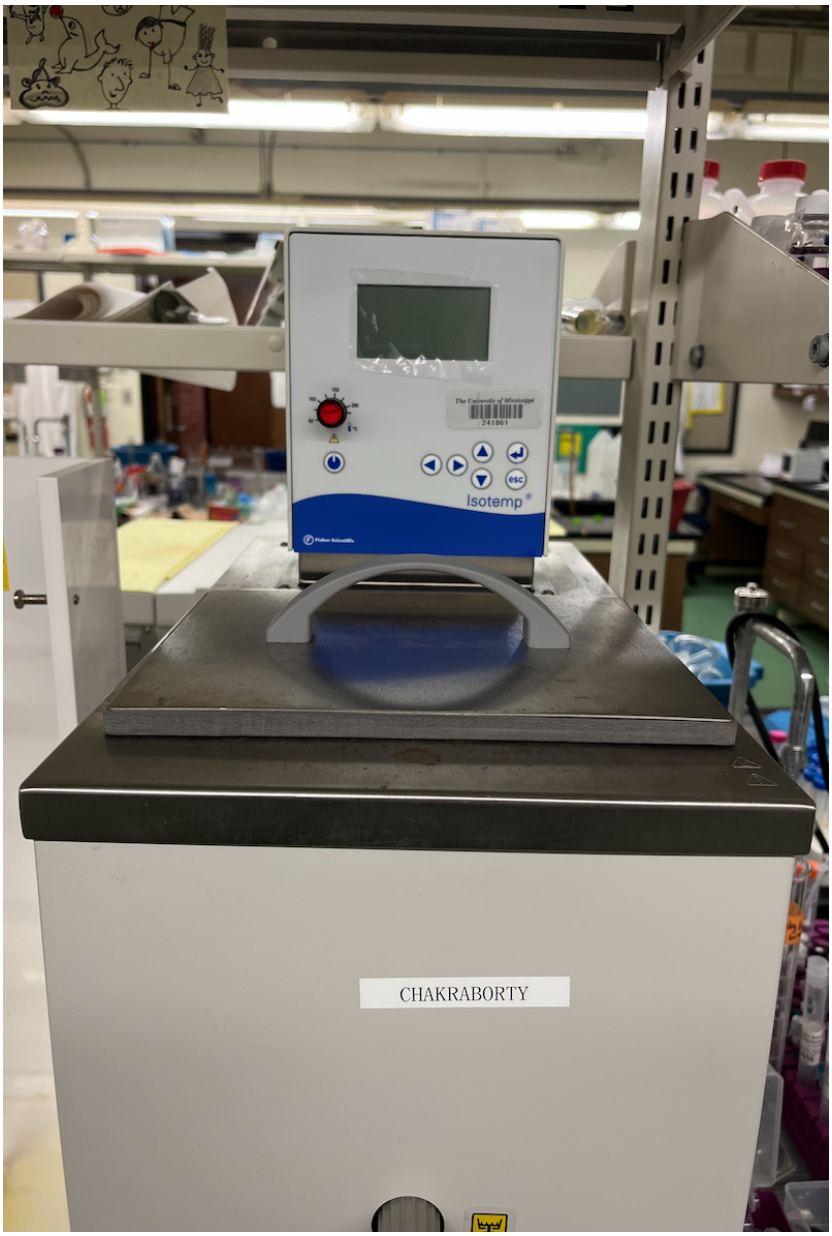

Image 5. Isotemp Aquastat

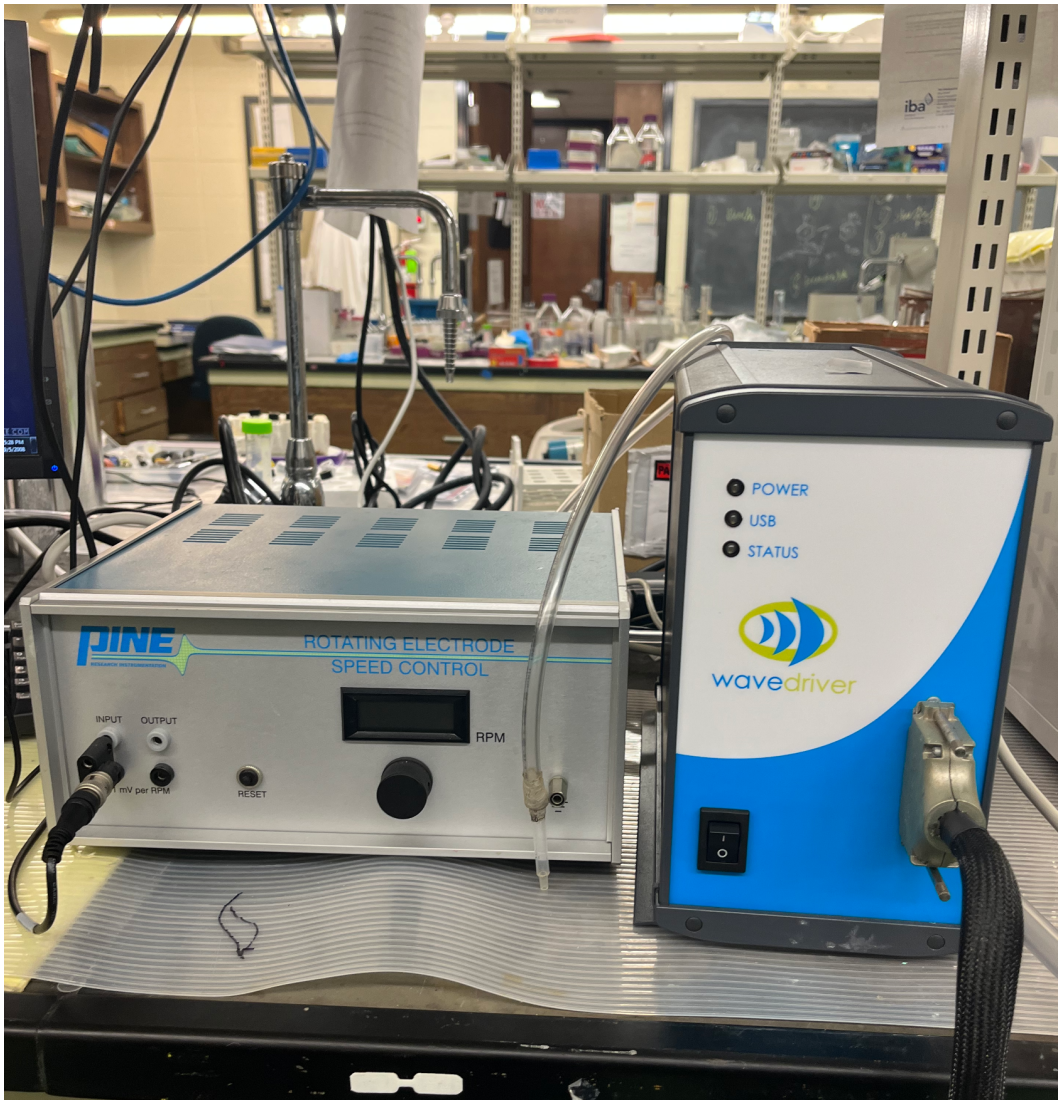

Image 6. Pine Wave Driver 20

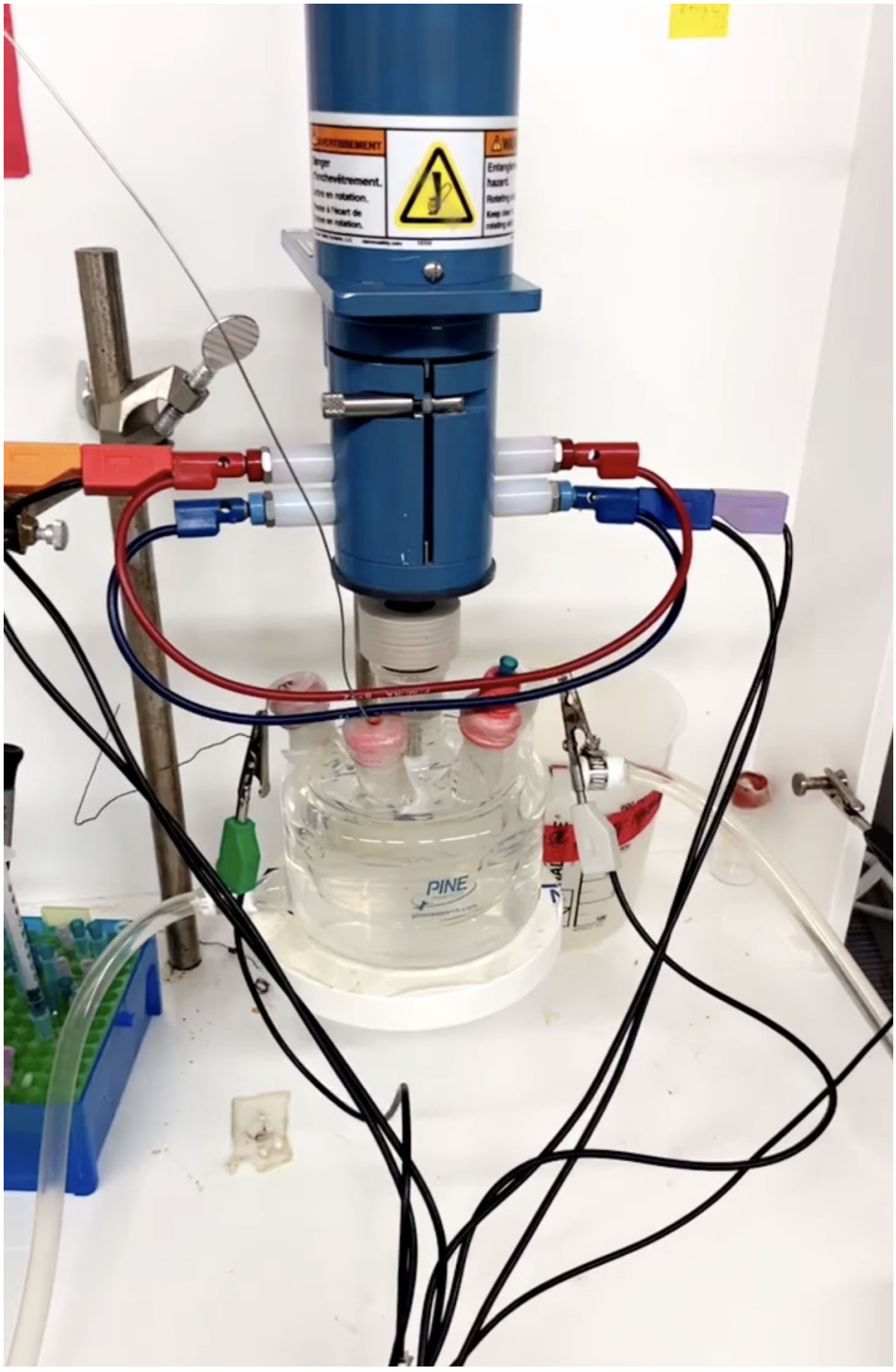

Image 7. Electrochemistry setup, white = Ag/AgCl reference electrode, green = platinum counter electrode, working electrode submerged in buffer solution

4.3 UV-Vis

To calculate the concentration of the Cu-peptide, UV-Visible spectroscopy is needed in conjunction with Beer's Law. In UV-vis spectroscopy there are two light sources, a deuterium source for the ultraviolet light which is in the range of 200-400 nm and a tungsten source for visible light from 400-800 nm. After the light source, the light enters the monochromator through the entrance slit, then reaches a dispersive device like a grating, then it goes through the exit slit, into the cuvette that contains the sample, excites in the electronic transition state, then goes to the detector to produce a spectra. When the light source reaches the sample, some of the energy of the light is absorbed by the sample, while other parts of the light are reflected. By parts of the light, certain wavelengths and colors are being referenced. When the sample absorbs light in the ultraviolet or visible region, the electrons are excited to an excited state which is an electronic transition. This is measured as the absorption. Certain characteristics of compounds absorb light at differing wavelengths, so different spectra reveal different structures present in the molecule. These are called chromophores, which are the functional groups that absorb light at specific wavelengths. The instrument used is the Cary 8454 Agilent UV-Vis spectrophotometer. It measures absorbance. UV-Vis spectroscopy is useful for biological macromolecules, transition metal ions, and conjugated compounds. It can also be used in conjunction with Beer's Law, $A = \varepsilon cl$, where A is absorbance, ε is the molar absorptivity coefficient, c is the concentration, and l is the path length in cm. [12]

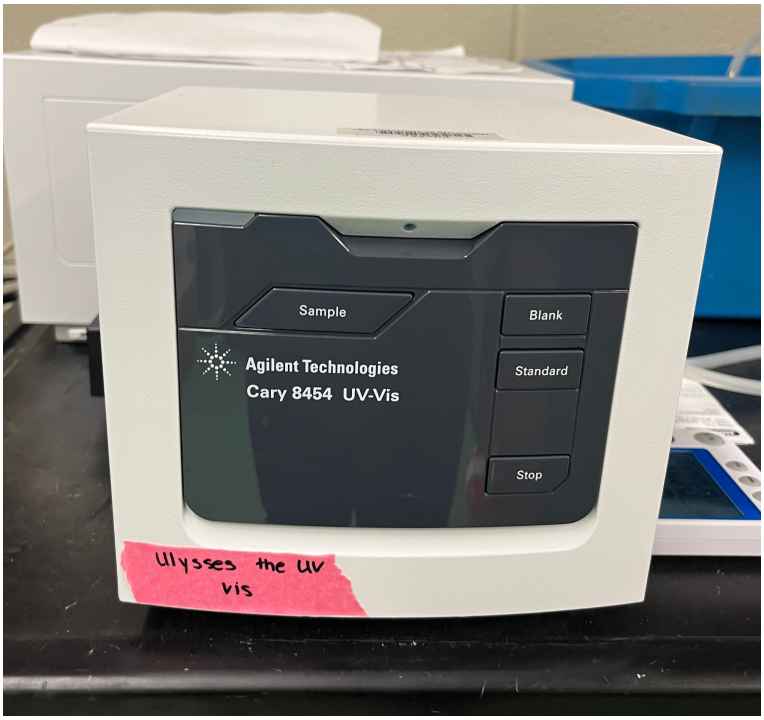

Image 8. Agilent Cary 8454 UV-Visible spectrophotometer

To measure the absorbance of the peptide, pure I2AA10W peptide was dissolved in 400 µL pH 6.5 MES buffer. Then, 2 µL of this dissolved peptide was added to a cuvette with 98 µL of MES buffer. The absorbance of this solution was measured. This value was then divided by the molar absorptivity coefficient of Trp which is 5500 $cm^{-1}M^{-1}$, and the peptide has an overall extinction coefficient of 5690 $cm^{-1}M^{-1}$ then multiplied by $\frac{98}{2}$ for the dilution factor, then this is the absorbance plugged into Beer's Law to solve for concentration.

After using the UV-Visible spectrophotometer to measure the absorbance of the stock peptide solution in 5 mM pH 6.5 MES buffer, Beer's Law was used to find the concentration of the stock solution. This was then used to calculate the volume of peptide, copper, and MES pH 6.5 buffer needed to create a 250 µM Cu-peptide solution for the I12AA10W mutant.

4.4 Temperature dependent CV

10 µL of the Cu-peptide solution was pipetted onto the PGE electrode and dried under a gentle flow of N_2 gas. Then 6 µL of Polymyxin B was pipetted and again dried under a gentle flow of N_2 gas. The Polymyxin B helps ensure the enzyme binds with the electrode. The cell is filled with 100 mL of pH 6.5 mixed buffer solution. The aquastat is set to the desired temperature for the temperature-dependent studies, ranging from 280 K to 310 K in 5 K increments. It takes around 15 to 20 minutes for the cell to reach the desired temperature. Next, the electrode is screwed into the electrochemical setup, lowered into the cell but not into the buffer, and purged in N_2 gas for five minutes before being lowered into the buffer.

After purging and lowering into the buffer, the nitrogen gas syringe was lifted out of the buffer to flow gently onto the buffer, but not bubble inside the cell, then the cyclic voltammetry was run at a sweep rate of 150 mV/s, with starting potential of 250 mV and lower potential of -250 mV, with a falling direction of the current. The CV was recorded in 4 segments. The surrounding area must be clean and without vibration, to avoid noise in spectra.

After running the cyclic voltammetry, the PGE was cleaned using a Kim wipe, followed by 1 µm alumina suspension and water on a polishing pad following a figure-eight motion, followed by sonication in MilliQ water for 10 minutes. Cleaning is important to avoid noise in spectra.

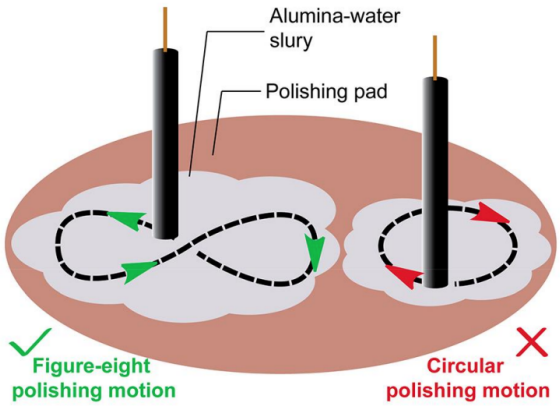

Figure 18. Method of cleaning the PGE electrode in figure-eight motion [1]

Image 9. 1 µm alumina suspension used for cleaning PGE

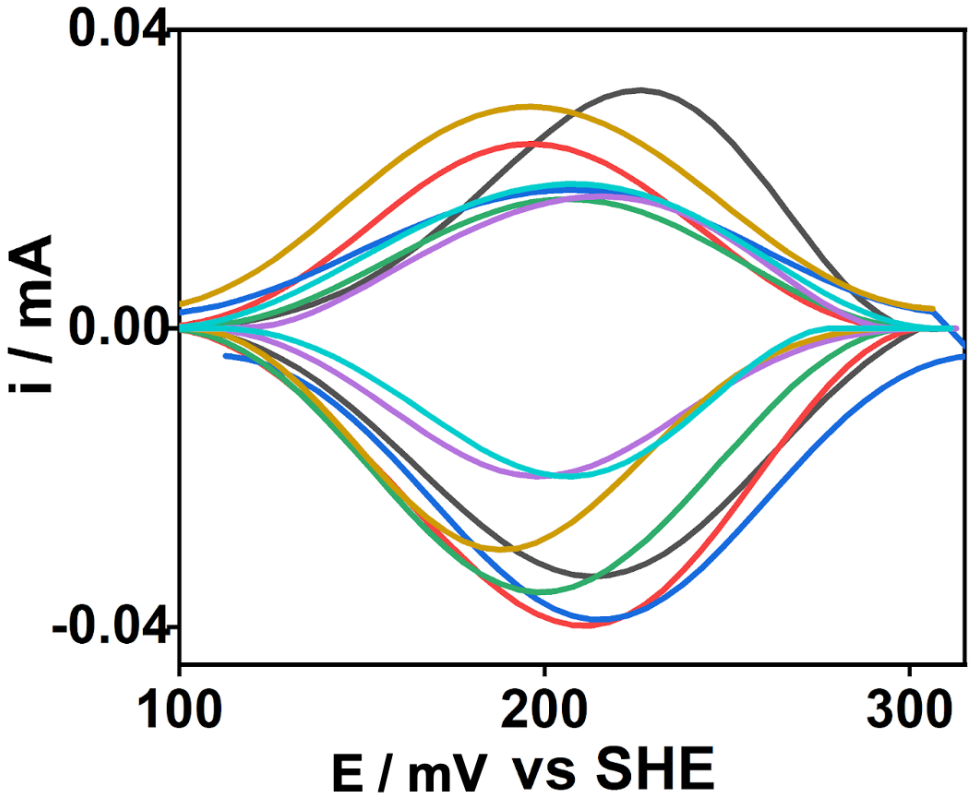

Figure 19. Temperature dependent CV of I12AA10W mutant performed at 280 K (black), 285 K (red), 290 K (blue), 295 K (green), 300 K (purple), 305 K (gold), and 310 K (cyan) at rate 150 mV/s; plotted in Origin

The small peak in the graph represents the binding of copper, and the reduction of Cu^{2+} to Cu^{+}. This is a way of confirming the binding of the copper to the peptide has occurred, as well as to the electrode. Data was exported from Pine and imported in QSOAS, where baseline corrections were completed for data at all temperatures. Data was then plotted in Origin in an overlay.

Temp	I_{pa} (μA)	E_{pa} (mV)	I_{pc} (μA)	E_{pc} (mV)	$E_{1/2}$ (mV)
280 K	31.9	229	-33.2	215	223
285 K	24.7	199	-39.7	210	205
290 K	18.6	209	-83.9	220	215
295 K	17.3	209	-35.3	200	206
300 K	17.6	219	-19.8	200	210
305 K	29.7	199	-29.6	191	195
310 K	19.4	209	-19.8	210	210

Table 4. I_{pa}, E_{pa}, I_{pc}, E_{pc} of temperature dependent CV of I12AA10W vs SHE

Furthermore, chronoamperometry (CA) experiments will be performed at negative and positive potentials with reference to the reduction potential, $E_{1/2}$ at various temperatures. The heterogeneous rate of electron transfer will be calculated using the equation of $i= kQ^{-(kt)}$, where k is heterogeneous rate of electron transfer, q is charge passed during chronoamperometry experiments and t is time.

Finally the Arrhenius equation will be used to determine the reorganization energy, λ, of $k=Ae^{-\frac{Ea}{RT}}$ where k is the rate constant, A is the Arrhenius constant, Ea is the activation energy, R is the gas constant, and T is temperature in Kelvin.

Chapter 5: Conclusion

In summary, copper enzymes play a large and important role in nature. By creating artificial copper peptides through de novo design and synthesis, there is a gain in understanding of the natural enzymes' mechanisms and behaviors. By studying de novo copper peptides in a variety of environments, mutations, reactions, and more, each step brings us closer to a full understanding of the abundant enzymes that surround us in nature. Inching closer to better

understanding is crucial for renewable energy sources and pharmaceutical research. We must continue to press forward in this field of research to reduce climate change and our carbon footprint. Future research would include fluorescence studies of the mutants in varying conditions, as well as studying other mutants.

References

[1] A practical beginner's guide to cyclic voltammetry. (n.d.). Retrieved April 17, 2023, from https://pubs.acs.org/doi/10.1021/acs.jchemed.7b00361

[2] Berry, John F. Department of Chemistry. (2023, January 20). Retrieved March 28, 2023, from https://chem.wisc.edu/staff/berry-john-f/

[3] Camp JV, Svensson TL, McBrayer A, Jonsson CB, Liljeström P, Bruder CE (2012) De-Novo Transcriptome Sequencing of a Normalized cDNA Pool from Influenza Infected Ferrets. PLoS ONE 7(5): e37104. https://doi.org/10.1371/journal.pone.0037104

[4] Hu, L. H., Farrokhnia, M., Heimdal, J., Shleev, S., Rulíšek, L., & Ryde, U. (2011). Reorganization energy for internal electron transfer in Multicopper oxidases. *The Journal of Physical Chemistry B*, *115*(45), 13111–13126. https://doi.org/10.1021/jp205897z

[5] International Flow Chemistry Equipment|Vapourtec Ltd. (n.d.). Retrieved March 28, 2023, from https://www.vapourtec.com/wp-content/uploads/2017/11/Automated-Peptide-Synthesis.pdf

[6] Klinman, J. P. (2005, November 21). *The copper-enzyme family of dopamine β-monooxygenase and peptidylglycine α-hydroxylating monooxygenase: Resolving the chemical pathway for substrate hydroxylation* *. Journal of Biological Chemistry. Retrieved April 17, 2023, from https://www.jbc.org/article/S0021-9258(20)81684-6/fulltext

[7] Le, T. H. (n.d.). *Artificial de novo tetramer hydrogenase mimic, co-metallopeptide titration, and photocatalysis*. eGrove. Retrieved March 28, 2023, from https://egrove.olemiss.edu/hon_thesis/1923/

[8] Mitra, S. (n.d.). *Exploring copper active sites in biology with relevance to alzheimer's disease and de novo designed biocatalysts*. eGrove. Retrieved March 28, 2023, from https://egrove.olemiss.edu/etd/2163/

[9] Mitra, S., Prakash, D., Rajabimoghadam, K., Wawrzak, Z., Prasad, P., Wu, T., Misra, S. K., Sharp, J. S., Garcia-Bosch, I., & Chakraborty, S. (2021, August 20). *De novo design of a self-assembled artificial copper peptide that activates and reduces peroxide*. ACS catalysis. Retrieved March 28, 2023, from https://www.ncbi.nlm.nih.gov/pmc/articles/PMC9524465/#SD1

[10] Mydy, L. S., Chigumba, D. N., & Kersten, R. D. (2021). Plant copper metalloenzymes as prospects for new metabolism involving aromatic compounds. *Frontiers in Plant Science*, *12*. https://doi.org/10.3389/fpls.2021.692108

[11] (PDF) chromatography in bioactivity analysis of compounds - researchgate. (n.d.). Retrieved March 28, 2023, from https://www.researchgate.net/publication/236146377_Chromatography_in_Bioactivity_Analysis_of_Compounds

[12] Prakash, D., Mitra, S., Murphy, M., & Chakraborty, S. (2022). Oxidation and peroxygenation of C–H bonds by artificial cu peptides (arcups): Improved catalysis via Selective Outer Sphere Modifications. *ACS Catalysis*, *12*(14), 8341–8351. https://doi.org/10.1021/acscatal.2c01882

[13] Prasad, P. (n.d.). *Re-engineered metalloproteins and rationally designed de novo peptides: Towards artificial hydrogenases*. eGrove. Retrieved March 28, 2023, from https://egrove.olemiss.edu/etd/2266/

[14] Skoog, D. A., Holler, J. F., & Crouch, S. R. (2018). *Principles of instrumental analysis*. Cengage Learning.

[15] Zerk, T. J., Saouma, C. T., Mayer, J. M., & Tolman, W. B. (2019). Low Reorganization Energy for Electron Self-Exchange by a Formally Copper(III,II) Redox Couple. *Inorganic chemistry*, *58*(20), 14151–14158. https://doi.org/10.1021/acs.inorgchem.9b02185